Newfound features of meiotic chromosome organization that promote efficient congression and segregation in *Caenorhabditis elegans* oocytes

Hannah H. Horton, Nikita S. Divekar, and Sarah M. Wignall*
Department of Molecular Biosciences, Northwestern University, Evanston, IL 60208

ABSTRACT **Although end-on microtubule–kinetochore attachments typically drive chromosome alignment, *Caenorhabditis elegans* oocytes do not form these connections. Instead, microtubule bundles run laterally alongside chromosomes and a ring-shaped protein complex facilitates congression (the "ring complex", RC). Here, we report new aspects of RC and chromosome structure that are required for congression and segregation. First, we found that in addition to encircling the outside of each homologous chromosome pair (bivalent), the RC also forms internal subloops that wrap around the domains where cohesion is lost during the first meiotic division; cohesin removal could therefore disengage these subloops in anaphase, enabling RC removal from chromosomes. Additionally, we discovered new features of chromosome organization that facilitate congression. Analysis of a mutant that forms bivalents with a fragile, unresolved homolog interface revealed that these bivalents are usually able to biorient on the spindle, with lateral microtubule bundles running alongside them and constraining the chromosome arms so that the two homologs are pointed to opposite spindle poles. This biorientation facilitates congression, as monooriented bivalents exhibited reduced polar ejection forces that resulted in congression defects. Thus, despite not forming end-on attachments, chromosome biorientation promotes congression in *C. elegans* oocytes. Our work therefore reveals novel features of chromosome organization in oocytes and highlights the importance of proper chromosome structure for faithful segregation during meiotic divisions.**

Monitoring Editor
Claire Walczak
Indiana University

Received: Jul 28, 2022
Revised: Sep 29, 2022
Accepted: Oct 3, 2022

INTRODUCTION

Meiosis is a specialized form of cell division used by sexually reproducing organisms to reduce their chromosome number by half to create haploid gametes. This reduction is accomplished by one round of DNA replication followed by two rounds of chromosome segregation. During Meiosis I, homologous partner chromosomes segregate away from one another to opposite spindle poles. To accomplish this, maternal and paternal homologs must first pair and become physically linked, forming bivalents. How the structure of meiotic bivalents impacts the fidelity of their segregation is poorly understood.

Physical linkage of homologous chromosomes is achieved when double-stranded DNA breaks are repaired via recombination to form a crossover (reviewed in Gray and Cohen, 2016; von Diezmann and Rog, 2021). *Caenorhabditis elegans* enacts strict crossover control, with exactly one double-stranded break repaired into a crossover per bivalent. This single crossover typically occurs off center along the chromosome axis, leading to the formation of long and short arms. The cohesin complex links sister chromatids on both the long and short arms of the bivalent; short-arm cohesion is removed

This article was published online ahead of print in MBoC in Press (http://www.molbiolcell.org/cgi/doi/10.1091/mbc.E22-07-0297) on October 12, 2022.

*Address correspondence to: Sarah M. Wignall (s-wignall@northwestern.edu).

Abbreviations used: APC, anaphase promoting complex; CPC, chromosome passenger complex; 3D-SIM, 3D structured illumination microscopy; MI, Meiosis I; MII, Meiosis II; MT, microtubule; RC, ring complex; RNAi, RNA interference; SUMO, small ubiquitin-like modifier.

during the first meiotic division to facilitate homolog segregation and long-arm cohesion is subsequently lost during the second meiotic division (reviewed in Schvarzstein *et al.*, 2010; Mullen *et al.*, 2019; Carlton *et al.*, 2022).

To ensure the specificity of cohesin loss during Meiosis I, chromosomes are remodeled during prophase so that the long- and short-arm domains differentially recruit factors that orchestrate cohesin loss on the short arm and protect cohesin on the long arm (Nabeshima *et al.*, 2005; de Carvalho *et al.*, 2008; Martinez-Perez *et al.*, 2008; Tzur *et al.*, 2012; Ferrandiz *et al.*, 2018; Sato-Carlton *et al.*, 2018). This patterning involves localization of the chromosomal passenger complex (CPC), which includes the conserved kinase AIR-2$^{\text{Aurora B}}$, to the short-arm domain. AIR-2 protects sister chromatid cohesion before anaphase and recruits the protease separase (SEP-1) to cleave cohesin upon anaphase onset (Kaitna *et al.*, 2002; Rogers *et al.*, 2002).

AIR-2 and other CPC components are also responsible for assembling a large ring-shaped structure that encircles the short-arm domain during Meiosis I and the sister chromatid interface during Meiosis II (Wignall and Villeneuve, 2009; Dumont *et al.*, 2010; Divekar *et al.*, 2021). This ring complex (RC) is made up of over a dozen proteins representing a diverse range of functional classes. These proteins assemble in a stepwise manner, with members of the CPC recruited first and other proteins, including the kinase BUB-1 and the kinesin-4 family member KLP-19, being targeted subsequently (Wignall and Villeneuve, 2009; Dumont *et al.*, 2010). The post-translational modification SUMO and its associated enzymes are also necessary for RC assembly and stability (Pelisch *et al.*, 2017; Davis-Roca *et al.*, 2018).

The RC plays important roles in *C. elegans* oocytes; depletion of RC proteins results in a variety of meiotic defects (Schumacher *et al.*, 1998; Romano *et al.*, 2003; Wignall and Villeneuve, 2009; Dumont *et al.*, 2010; Connolly *et al.*, 2015; Laband *et al.*, 2017; Pelisch *et al.*, 2017, 2019; Divekar *et al.*, 2021), and univalents without RCs are unable to achieve proper metaphase alignment (Muscat *et al.*, 2015). Notably, chromosome congression in *C. elegans* oocytes is mediated by a unique mechanism that does not require end-on kinetochore–microtubule attachments. Instead, microtubule bundles run laterally along the sides of chromosomes, forming channels that chromosomes move through (Wignall and Villeneuve, 2009; Redemann *et al.*, 2018). This movement depends upon KLP-19, which has been proposed to walk toward the plus ends of these laterally associated microtubules, thus generating an anti-poleward "polar ejection" force necessary to achieve alignment at the metaphase plate (Wignall and Villeneuve, 2009). During anaphase, the RCs dissociate from chromosomes and remain at the center of the spindle within the microtubule channels briefly before disassembling (Dumont *et al.*, 2010; Muscat *et al.*, 2015; Davis-Roca *et al.*, 2017; Mullen and Wignall, 2017; Davis-Roca *et al.*, 2018). However, RC disassembly is delayed under experimental conditions that induce defects in chromosome segregation, suggesting the presence of a regulatory mechanism that slows aspects of anaphase progression in response to errors (Davis-Roca *et al.*, 2017).

While this previous work has characterized the various functions of the RC, how the RC's structural properties confer its function remains to be understood. Here, we report additional insights into the structure and organization of this important protein complex. Using superresolution imaging, we discovered a new domain of the RC that weaves through the center of the Meiosis I bivalent. We went on to analyze mutants with defective chromosome structure, revealing new insights into how defects in chromosome organization and ring structure have consequences for the fidelity of the meiotic divisions. Altogether, these experiments shed light on the organizing principles of these essential structures.

RESULTS AND DISCUSSION

The ring complex contains internal subloops

The original discovery of the RC identified a structure that wrapped around the mid-bivalent region in Meiosis I and the sister chromatid interface in Meiosis II, leading to the conceptualization of this protein complex as a hollow ring-shaped structure (Wignall and Villeneuve, 2009). However, we have observed that when the RC is imaged from an end-on view, a more intricate structure can be seen. Specifically, using immunofluorescence, we found that AIR-2$^{\text{Aurora B}}$, a kinase and core RC component, weaves through the central region of the Meiosis I bivalent in addition to encircling the bivalent's outer surface, revealing a structure more complex than originally modeled (Figure 1A, arrow). Interestingly, while AIR-2 was observed in this interwoven structure in 100% of Meiosis I bivalents (57/57 bivalents), we were unable to observe this feature when imaging the RC from an end-on view during Meiosis II (0/54 bivalents), suggesting that these structures are specific to the Meiosis I bivalent (Figure 1A).

We also stained for the posttranslational modification SUMO and found it localized to the internal region of the Meiosis I bivalent as well (Figure 1A). Since SUMO facilitates the targeting of multiple other proteins to the RC, we hypothesized that additional components would therefore also be found in the internal structures. For example, the kinase BUB-1 and the chromokinesin KLP-19 require SUMO for recruitment to the RC (Pelisch *et al.*, 2017). However, both BUB-1 and KLP-19 localize to additional niches on the bivalent, with BUB-1 occupying the kinetochore (Dumont *et al.*, 2010; Supplemental Figure S1A) and KLP-19 diffusely occupying the chromatin (Pelisch *et al.*, 2017; Supplemental Figure S1B). When staining with antibodies for these proteins, these additional localizations impeded observation of internal ring structure. Therefore, we reduced the localization of non-RC BUB-1 by partially knocking down the kinetochore protein KNL-1 (Supplemental Figure S1A). Moreover, we found that the chromatin-associated population of KLP-19 could be removed by knocking down the CENP-C homolog HCP-4 (which also localizes to the chromosome arms; Monen *et al.*, 2005), demonstrating that HCP-4 is required for targeting proteins to this region of the bivalent (Supplemental Figure S1B). These conditions enabled us to detect BUB-1 and KLP-19 in the internal interwoven structures in Meiosis I (Supplemental Figure S1, C and D), demonstrating that multiple RC components are found in this structure and suggesting that the organization of the RC is more elaborate than previously appreciated.

To visualize this novel structure more clearly, we conducted superresolution 3D structured illumination microscopy (3D-SIM). We immunostained oocytes using antibodies against AIR-2 and SUMO and visualized Meiosis I bivalents from an end-on orientation. This increased resolution revealed that the RC contains two distinct subloops within the larger structure (Figure 1B, arrows). To get a better view of these features, we took advantage of a published RC stretching assay. Previously, we found that when spindles are arrested in metaphase for an extended period of time using a temperature-sensitive mutant in a component of the Anaphase Promoting Complex (APC; *emb-27(g48)*), the RCs stretch off the chromosomes toward the plus ends of the microtubules (Muscat *et al.*, 2015). We reasoned that this stretching might draw the outer portion of the RC away from the chromosome, allowing a better view of the internal structure. The stretching effect is exaggerated on a monopolar spindle, where all the minus ends form a single pole, since each RC is

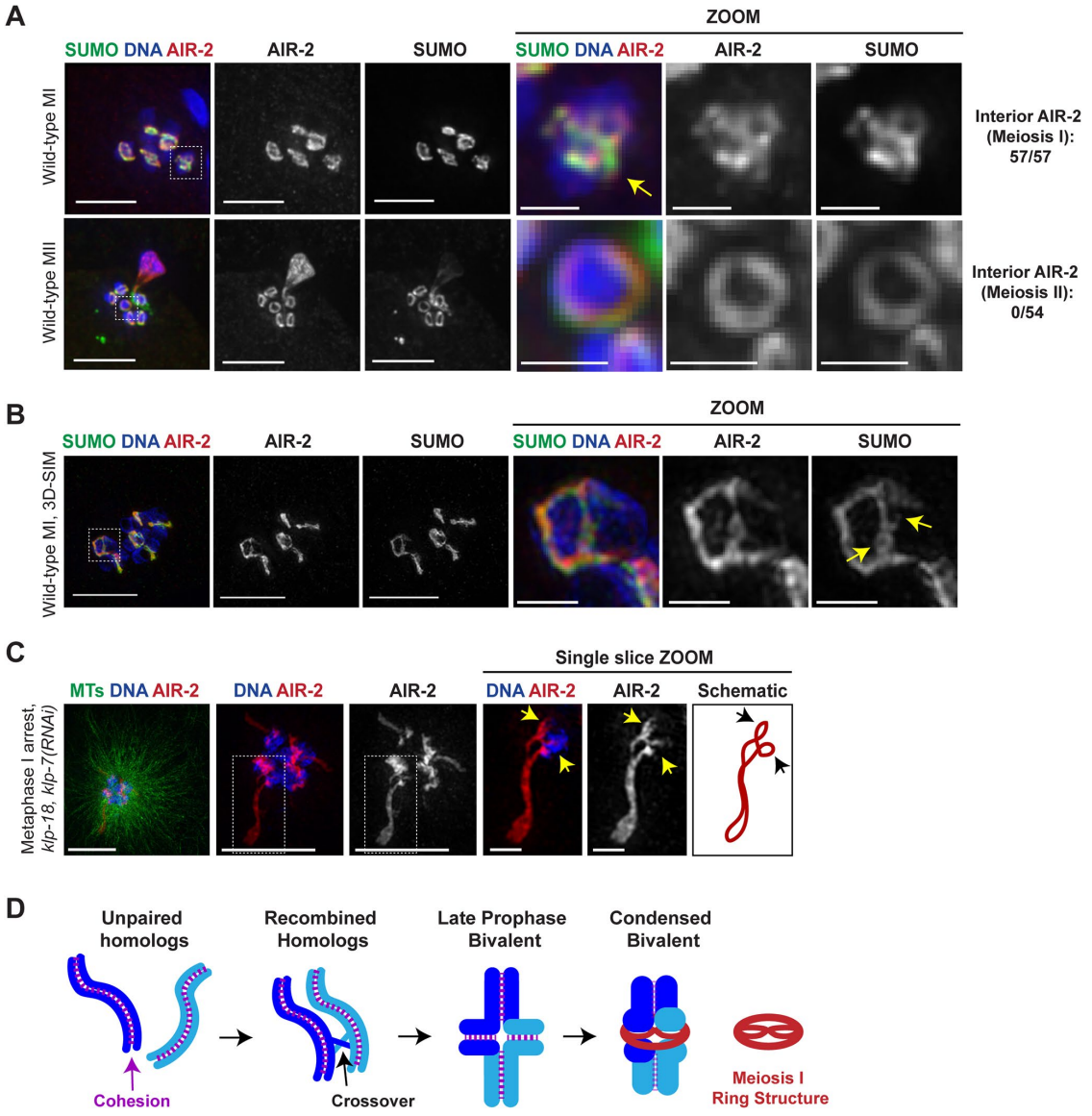

FIGURE 1: The ring complex has internal domains that weave through Meiosis I bivalents. (A) Meiosis I bivalents (Top) and Meiosis II chromosomes (Bottom); shown are DNA (blue), SUMO (green), and AIR-2 (red). Zooms highlight individual RCs; MI bivalents have an internal substructure (arrow; 57/57) while MII chromosomes do not (0/54 have internal RC components). (B) 3D-SIM superresolution image of an end-on Meiosis I bivalent; shown are DNA (blue), SUMO (green), and AIR-2 (red). Arrows highlight subloops within the RC. (C) 3D-SIM superresolution image of a Metaphase I-arrested monopolar spindle. This condition was generated by performing *klp-18;klp-7*^{MCAK}*(RNAi)* in *emb-27(g48)ts* worms and shifting them to the restrictive temperature. AIR-2 (red) stretches toward the plus ends of the microtubules, which reveals subloops (arrows) associated with the bivalent; subloops are apparent in the single-slice zoom (schematic shows RC organization). (D) Model for RC organization in Meiosis I. Homologous chromosomes are shown in light/dark blue and cohesin linking sisters is shown in purple. After homologs pair and a single off-centered crossover occurs, the cruciform structure condenses such that the short arms are indistinguishable from the long arms. The RC (red) forms subloops around the short arms of the bivalents as well as encircling the outside of the bivalent. Scale bars = 5 μm (full images), 1 μm (zooms).

pulled outward in one direction toward the plus ends. Moreover, knocking down the microtubule depolymerizer KLP-7^{MCAK} leads to the formation of larger monopolar spindles, further exaggerating the stretching (Muscat *et al.*, 2015). Under these conditions, RC components stretched toward the plus ends of the microtubules as expected. Notably, this revealed two distinct subloops weaving through the center of the bivalent (Figure 1C, arrows, Movie 1); we infer that these are the subloop structures previously seen in end-on imaging of unstretched RCs (Figure 1B).

Taken together, this imaging has enhanced our understanding of bivalent organization by revealing distinct domains within the RC during Meiosis I. Given the location of the subloops in the central region of the bivalent, we hypothesize that the RC weaves around the bivalent short arms, which are condensed and indistinguishable from the long arms (Figure 1D). Furthermore, the persistence of the subloops during the RC stretching assay suggests that these structures may serve as physical contact points between the bivalent and the RC, helping to connect the RCs to the bivalent in Meiosis I.

Chromosome structure mutants exhibit defects in ring complex organization

To better understand the relationship between the RC's intricate structure and its function, we sought to examine the effects of perturbations in RC structure caused by altered bivalent organization. First, we examined RC structure in an *akir-1(rj1)* mutant with defects in synaptonemal complex disassembly, resulting in an enlarged gap between the two bivalent lobes (Clemons *et al.*, 2013). Despite these changes to the central region of the bivalent, RC organization appeared similar to wild type; the interwoven subloop feature of the RC was apparent, further confirming the internal localization of RC components (Figure 2A). Second, we assessed a *him-18(tm2181)* mutant with incomplete Holliday Junction resolution, resulting in the homologs being linked by a hemicatenane (two DNA duplexes linked with a single-strand interlock) instead of a mature crossover; this defect causes the two bivalent lobes to be "cracked open," exposing the mid-bivalent region (Saito *et al.*, 2009; Figure 2, A and B). We found that RC components loaded onto the exposed inner surfaces of the bivalent lobes (Figure 2A), as previously reported for AIR-2 (Saito *et al.*, 2009). When looking closely at *him-18(tm2181)* bivalents, we noticed a small DNA body adjacent to each lobe of the cracked-open bivalent (Figure 2B, arrows). We hypothesized that these "nubs" were the short arms, which are normally condensed and tucked into the mid-bivalent region but would be exposed if the bivalent were cracked open. Interestingly, AIR-2 and SUMO wrapped around these putative short arms, forming a loop around each (Figure 2B), supporting our hypothesis that the subloop structures within the RC wrap around the short arms of the Meiosis I bivalent. Notably, these subloops were the predominant feature in *him-18(tm2181*) cracked-open bivalents (Figure 2B), and we did not detect a larger ring encircling the outside of the structure (as seen in wild type; Figure 1D). This observation may imply that this outer ring can only form when the short-arm interface of the bivalent is properly formed, though further analysis would be needed to test this hypothesis.

To determine how the kinetochore was affected by altered bivalent structure, we stained for the kinetochore protein CLS-2^{CLASP} on *him-18(tm2181)* bivalents. Because *C. elegans* chromosomes are holocentric, kinetochores assemble along the surface of wild-type bivalents, appearing as a cuplike structure (Monen *et al.*, 2005; Dumont *et al.*, 2010; Figure 2C, Top). While kinetochore proteins do not typically load onto the short arms, we noticed that all exposed surfaces of cracked-open *him-18(tm2181)* bivalents, including the short arms, were coated in CLS-2 (71/71 bivalents; Figure 2C). This observation suggests that kinetochore proteins will load onto any exposed region of the chromosome, demonstrating the importance of bivalent organization in occluding the short arms from erroneous protein localization.

Biorientation is required for proper congression of bivalents

Previous work has indicated that chromosomes lacking RCs do not properly congress in *C. elegans* oocytes (Muscat *et al.*, 2015). Furthermore, chromosomes that exhibit too many crossovers assemble aberrantly shaped RCs that are unable to facilitate chromosome congression, suggesting that the structure of the RC affects its function (Hollis *et al.*, 2020). To further probe this idea, we assessed the ability of bivalents to align at the metaphase plate in *akir-1* and *him-18* mutants. To quantify congression, we pinpointed the location of each RC within the spindle; we then measured the distance between the two most poleward RCs and divided it by the length of the spindle to generate a ratio that approximated the degree of chromosome alignment at the metaphase plate (Figure 3A). When wild-type spindles were arrested in metaphase using RNAi-mediated depletion of APC component EMB-30, chromosomes aligned tightly at the spindle center, resulting in a low metaphase plate ratio (0.20, n = 15; Figure 3A). Interestingly, a similar ability of chromosomes to align was seen in *akir-1(rj1)* spindles (0.26, n = 25), consistent with the fact that chromosome and RC organization do not appear to be substantially altered in this mutant (Figure 2A). In contrast, chromosomes in the *him-18* mutant occupied a larger fraction of the spindle, indicating problems with chromosome alignment (0.43, n = 25; Figure 3A). Because this quantification method accounted only for the most anomalous bivalents on each spindle, we also measured the distance between each individual RC and the nearest pole. We then divided this distance by the spindle length in order to pinpoint the position of each bivalent; a perfectly aligned bivalent would have a ratio of 0.5 (corresponding to the spindle center), while shorter migration distances would yield lower ratios. We found that these bivalent migration ratios comported with our spindlewide assessment of alignment; while robust alignment was seen for both wild-type bivalents (mean = 0.47, n = 88) and *akir-1(rj1)* bivalents (0.47, n = 116), many *him-18(tm2181)* bivalents were located further from the metaphase plate (0.38, n = 110; Figure 3A).

Interestingly, when assessing congression in the *him-18* mutant, we noticed that the orientation of the bivalent lobes relative to the pole-to-pole spindle axis often varied between bivalents on the same spindle. A majority of *him-18(tm2181)* bivalents were oriented similarly to wild-type, with the two lobes pointing toward opposite poles and the RC situated between the lobes; these bivalents were thus able to biorient on the spindle (141/184 bivalents; 76.6%; Figure 3B, zoom 1). In contrast, some bivalents had both lobes oriented toward a single pole with the RC and the exposed short arms facing the opposite pole; these bivalents were thus monooriented (43/184 bivalents; 23.4%; Figure 3B, zoom 2). Based on these observations, we categorized *him-18(tm2181)* bivalents into one of two classes: (1) "stacked" bivalents, where the two lobes were oriented in opposite directions and stacked on top of each other, or (2) "cracked" bivalents, which were fully cracked open and had both lobes pointing in the same direction (Figure 3B).

Given the major alignment defects in *him-18* mutant spindles, we next wondered whether stacked and cracked bivalents differed in their ability to congress. Notably, individual *z*-slices of *him-18* mutant spindles revealed that both types of bivalents appeared to be ensheathed in laterally associated microtubule bundles (Figure 3B; Movie 2), which could potentially enable them to migrate along those bundles to align at the metaphase plate. Therefore, to determine if these bivalents were capable of this type of migration, we assessed chromosome positioning on a monopolar spindle. Monopolar spindles have a single pole with microtubule plus ends oriented outward; chromosomes in wild-type oocytes travel to the plus ends, a movement analogous to chromosome congression on a bipolar spindle (Wignall and Villeneuve, 2009; Muscat *et al.*, 2015; Hollis *et al.*, 2020). Depletion of the RC-localized motor KLP-19 results in a failure of chromosomes to migrate outward on a monopolar spindle, confirming that it is needed to generate this polar ejection force (Wignall and Villeneuve, 2009).

We therefore used this assay to compare the plus end–directed migration of wild-type, *him-18* stacked, and *him-18* cracked bivalents by measuring the distance between the center of the monopole (designated by the microtubule minus-end marker ASPM-1) and the poleward-most surface of the bivalent (Figure 3C). Wild-type bivalents moved away from the pole an average distance of 2.83 ± 0.07 μm (n = 99; Figure 3C). Notably, stacked *him-18* bivalents migrated at distances similar to control bivalents (2.79 ± 0.11 μm,

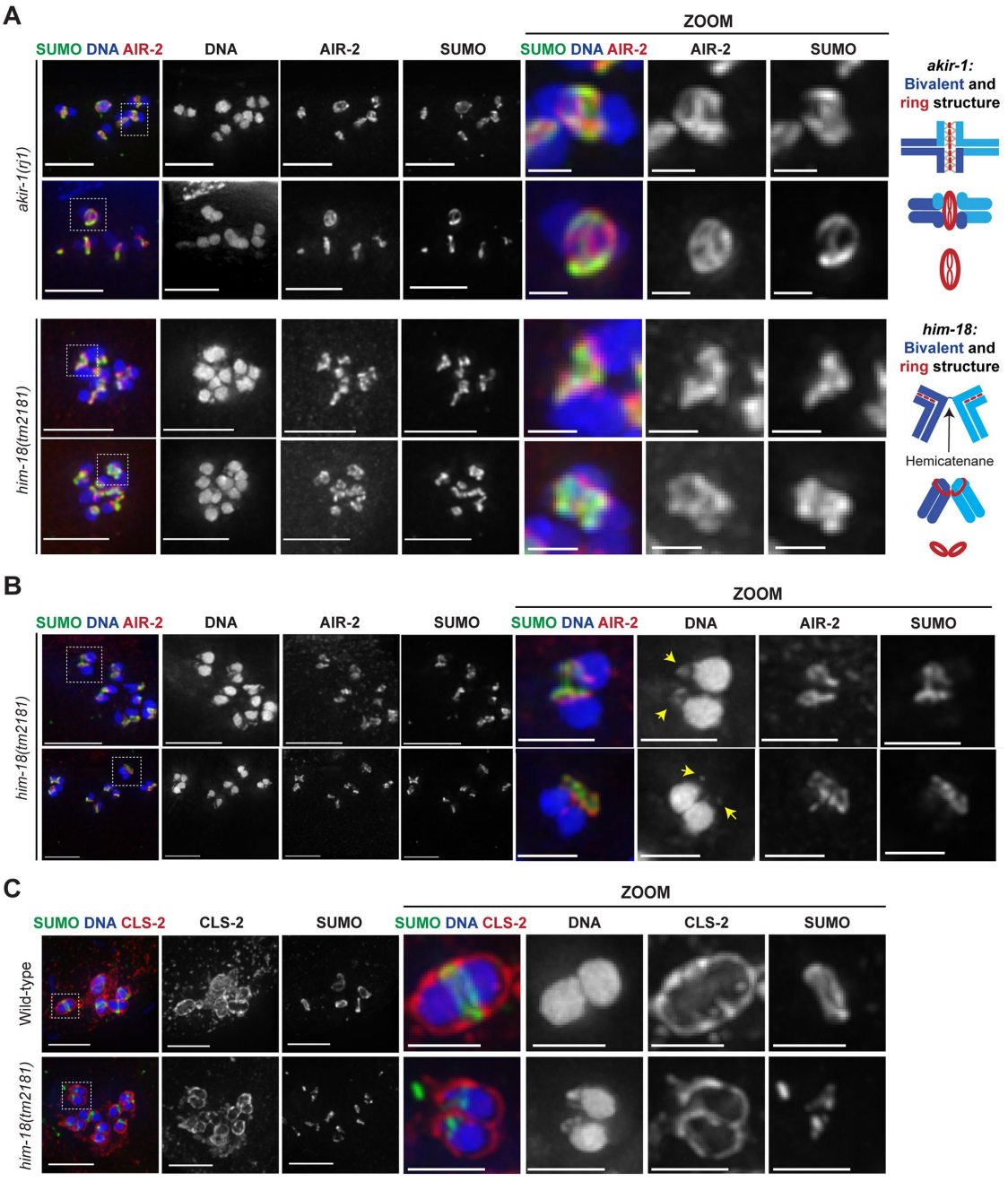

FIGURE 2: Chromosome structure mutants exhibit defects in bivalent and ring complex organization. (A) Meiosis I bivalents in *akir-1(rj1)* and *him-18(tm2181)* mutants; shown are DNA (blue), SUMO (green), and AIR-2 (red). Zooms of individual bivalents show RC structure in each mutant; diagrams detailing bivalent and ring structure are shown to the right of the images. Bivalents in the *akir-1* mutant have a large gap in the center, highlighting the interwoven subloop structure. In *him-18* mutants, bivalents are cracked open; top row shows a cracked bivalent from the side, and the bottom row shows a top view. (B) Additional examples of *him-18(tm2181)* cracked-open bivalents; shown are DNA (blue), SUMO (green), and AIR-2 (red). Zooms of individual chromosomes show the cracked-open structure of *him-18* bivalents with short-arm "nubs" exposed (arrows). RC components loop around these nubs, forming collars. (C) Meiosis I bivalents in wild-type oocytes (top) and *him-18(tm2181)* mutants (bottom); shown are DNA (blue), SUMO (green), and CLS-2 (red). CLS-2 localizes to the kinetochores of wild-type bivalents and coats the exposed short arms of cracked-open *him-18(tm2181)* bivalents, which are usually inaccessible. Scale bars = 5 μm (full images), 1 μm (zooms).

$n = 59$), while the migration distance of cracked *him-18* bivalents was nearly 1.6-fold lower than either stacked *him-18* or control distances (1.79 ± 0.05 μm, $n = 87$; Figure 3C). Therefore, cracked bivalents exhibit defects in plus end–directed migration, suggesting that the altered positioning of the RC to one end of the bivalent may affect its ability to generate a polar ejection force. Thus, proper placement of the RC at the center of the two bivalent lobes is likely important for efficient congression. Interestingly, we also found that the cracked bivalents were oriented nonrandomly on monopolar spindles; more bivalents (83/93; 89.25%) were oriented with their RCs pointing

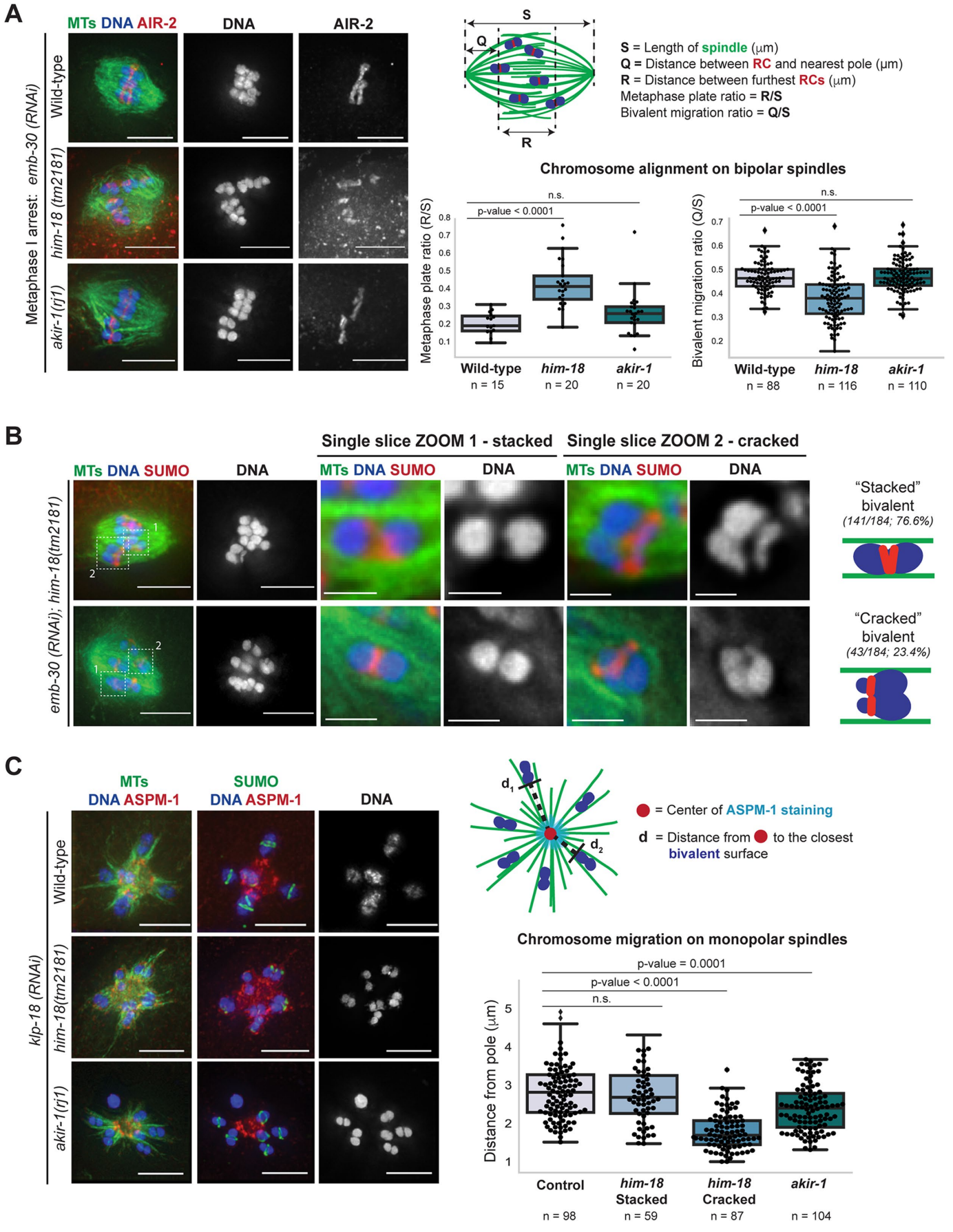
A
MTs DNA AIR-2
DNA
AIR-2
Metaphase I arrest: emb-30 (RNAi)
Wild-type
him-18 (tm2181)
akir-1(rj1)
S
Q
R
S = Length of spindle (μm)
Q = Distance between RC and nearest pole (μm)
R = Distance between furthest RCs (μm)
Metaphase plate ratio = R/S
Bivalent migration ratio = Q/S
Chromosome alignment on bipolar spindles
Metaphase plate ratio (R/S)
n.s.
p-value < 0.0001
Wild-type n = 15
him-18 n = 20
akir-1 n = 20
Bivalent migration ratio (Q/S)
n.s.
p-value < 0.0001
Wild-type n = 88
him-18 n = 116
akir-1 n = 110
B
Single slice ZOOM 1 - stacked
Single slice ZOOM 2 - cracked
MTs DNA SUMO
DNA
emb-30 (RNAi); him-18(tm2181)
"Stacked" bivalent (141/184; 76.6%)
"Cracked" bivalent (43/184; 23.4%)
C
MTs DNA ASPM-1
SUMO DNA ASPM-1
DNA
klp-18 (RNAi)
Wild-type
him-18(tm2181)
akir-1(rj1)
d1
d2
= Center of ASPM-1 staining
d = Distance from to the closest bivalent surface
Chromosome migration on monopolar spindles
Distance from pole (μm)
p-value = 0.0001
p-value < 0.0001
n.s.
Control n = 98
him-18 Stacked n = 59
him-18 Cracked n = 87
akir-1 n = 104

outward, toward the microtubule plus ends. This observation is consistent with previous work demonstrating that the RC provides a plus end–directed force (Wignall and Villeneuve, 2009; Muscat *et al.*, 2015), and suggests that, when the RC is located off center, it may preferentially pull the cracked bivalents toward the plus ends, with the DNA lobes trailing behind, rather than push the bivalent from the back of the structure.

Curiously, *akir-1* bivalents traveled a slightly shorter distance than control bivalents toward the plus ends on monopolar spindles (2.44 ± 0.07 μm compared with 2.83 ± 0.07 μm; Figure 3C) despite not exhibiting significant congression defects on a bipolar spindle (Figure 3A). Therefore, *akir-1(rj1)* bivalents may be slightly less efficient at generating a polar ejection force, but this does not appreciably impact their ability to congress. Notably, the distance traveled by the *akir-1(rj1)* bivalents is still substantially greater than that for *him-18* cracked bivalents, consistent with an advantage of wild-type bivalent lobe orientation in chromosome congression. Thus, these data suggest a requirement for proper distribution of bivalent mass relative to the RC in chromosome congression, with imbalanced bivalents displaying less polar ejection force even when lateral bundles are present.

Defects in chromosome structure cause chromosome segregation errors

Given the chromosome orientation and congression defects in *him-18(tm2181)* mutants, we next sought to assess the consequences for chromosome segregation. A previous study reported lagging chromosomes and chromosome bridges in this mutant during Anaphase I (9/15 spindles; 60%; Saito *et al.*, 2009), and we observed a similar number of late anaphase defects (13/20; 65%; Figure 4A), confirming that there are frequent problems with chromosome segregation. Therefore, we sought to assess anaphase in this mutant carefully, to better understand the nature of these defects.

In control spindles, the protease separase (SEP-1) relocalizes from the kinetochores to the RCs at anaphase onset (Muscat *et al.*, 2015; Supplemental Figure S2, A and B). Cohesin is then released along the short-arm interface, enabling chromosomes to separate (Kaitna *et al.*, 2002; Rogers *et al.*, 2002). RCs detach from the chromosomes and initially remain in the center of the spindle in early anaphase. RC components are then progressively removed from these structures and the complexes disassemble, with AIR-2 and SUMO relocalizing to the spindle by late anaphase (Davis-Roca *et al.*, 2017, 2018; Pelisch *et al.*, 2019).

To determine if these events still occur in *him-18* mutants, we first assessed early anaphase spindle organization by depleting MEL-28, a nucleoporin necessary for anaphase progression (Hattersley *et al.*, 2016). Depletion of MEL-28 causes an early anaphase arrest; the spindle shortens, SEP-1 relocalizes to the RC, chromosomes separate a short distance, and the RCs remain intact in the center of the spindle (Hattersley *et al.*, 2016; Davis-Roca *et al.*, 2018; Figure 4B; Supplemental Figure S2B). In these spindles, there is a gap between the RCs and the sets of separating chromosomes, indicating that the RCs have detached from the chromosomes (Figure 4B, zoom).

Interestingly, we found that RCs in the *him-18* mutant did not dissociate properly from bivalents but instead remained associated with segregating chromosomes in early anaphase, stretching between the homologs (Figure 4B, Movie 3); careful observation revealed that the RCs were still looped around the short-arm "nubs" that extended away from the rest of the chromosome (Figure 4B, zooms). We quantified this phenotype by measuring the fraction of the anaphase spindle occupied by RCs following *mel-28(RNAi)* (Figure 4C); RCs occupied a larger fraction of the spindle in *him-18(tm2181)* than of wild-type spindles (0.64 ± 0.04 compared with 0.49 ± 0.03), consistent with the fact that some RCs failed to disjoin and therefore stretched across the entire spindle. Notably, we confirmed that SEP-1 localized normally to the kinetochores in *him-18(tm2181)* prometaphase spindles and then was found at the midzone of *him-18(tm2181), mel-28(RNAi)* spindles (Supplemental Figure S2, A and B), confirming that these are *bona fide* anaphase spindles.

These results suggest that the chromosome structure defects in *him-18* mutants interfere with RC release. In wild-type bivalents, the internal subloops of the RC appear to wrap around the short-arm interface, where the cohesin complex links sisters (Figure 1D); thus,

FIGURE 3: Bivalents with monooriented long arms exhibit defects in chromosome migration on the spindle. (A) Wild-type (EU1067), *him-18(tm2181)* and *akir-1(rj1)* Meiosis I spindles arrested in metaphase via *emb-30(RNAi);* shown are DNA (blue), tubulin (green), and AIR-2 (red). Chromosome alignment was calculated by measuring the distance between the two most poleward rings (R) and then dividing that distance by the pole-to-pole length of the spindle (S). There are defects in bivalent alignment in *him-18(tm2181)* spindles compared with wild-type (p value = 4.73×10^{-7}; two-tailed Student's t test), but no significant defects in *akir-1(rj1)* mutants ($p = 0.09$). Additionally, the distance between each RC and its nearest pole was measured (Q) and divided by spindle length (S) to assess individual chromosomes; a value of 0.5 means a chromosome is at the center of the spindle, whereas a smaller value denotes a chromosome located closer to a pole. Note that some values are above 0.5 since the measurements were made on 3D renderings of each spindle; if a chromosome was found above or below the pole-to-pole spindle axis, the distance was measured at an angle, sometimes resulting in a measurement greater than half of the pole-to-pole distance. There are defects in bivalent alignment in *him-18(tm2181)* spindles compared with wild-type (p value = 3.80×10^{-13}; two-tailed Student's t test), but no significant defects in *akir-1(rj1)* mutants ($p = 0.76$). (B) Meiosis I *him-18(tm2181)* spindles arrested in metaphase via *emb-30(RNAi);* shown are DNA (blue), tubulin (green), and SUMO (red). Single-slice zooms show examples of "stacked" bivalents (zoom 1; left), where the bivalent lobes are pointed to opposite spindle poles, and "cracked" bivalents (zoom 2; right), where the bivalent is monooriented with the RC toward one spindle pole and both bivalent lobes toward the other. (C) Wild-type (EU1067), *him-18(tm2181)* and *akir-1(rj1)* monopolar spindles generated by *klp-18(RNAi);* shown are DNA (blue), tubulin (green, column 1), SUMO (green, column 2), and ASPM-1 (red). Chromosome migration distances were measured from the center point of the ASPM-1 volume to the poleward face of each bivalent. Migration of stacked *him-18* bivalents was not significantly different from wild-type bivalents ($p = 0.78$; two-tailed Student's t test), while *him-18* cracked bivalents did not migrate as far ($p < 8.66 \times 10^{-23}$). *akir-1(rj1)* bivalents had a small but significant migration defect compared with wild-type ($p = 0.0001$). Scale bars = 5 μm (full images), 1 μm (zooms).

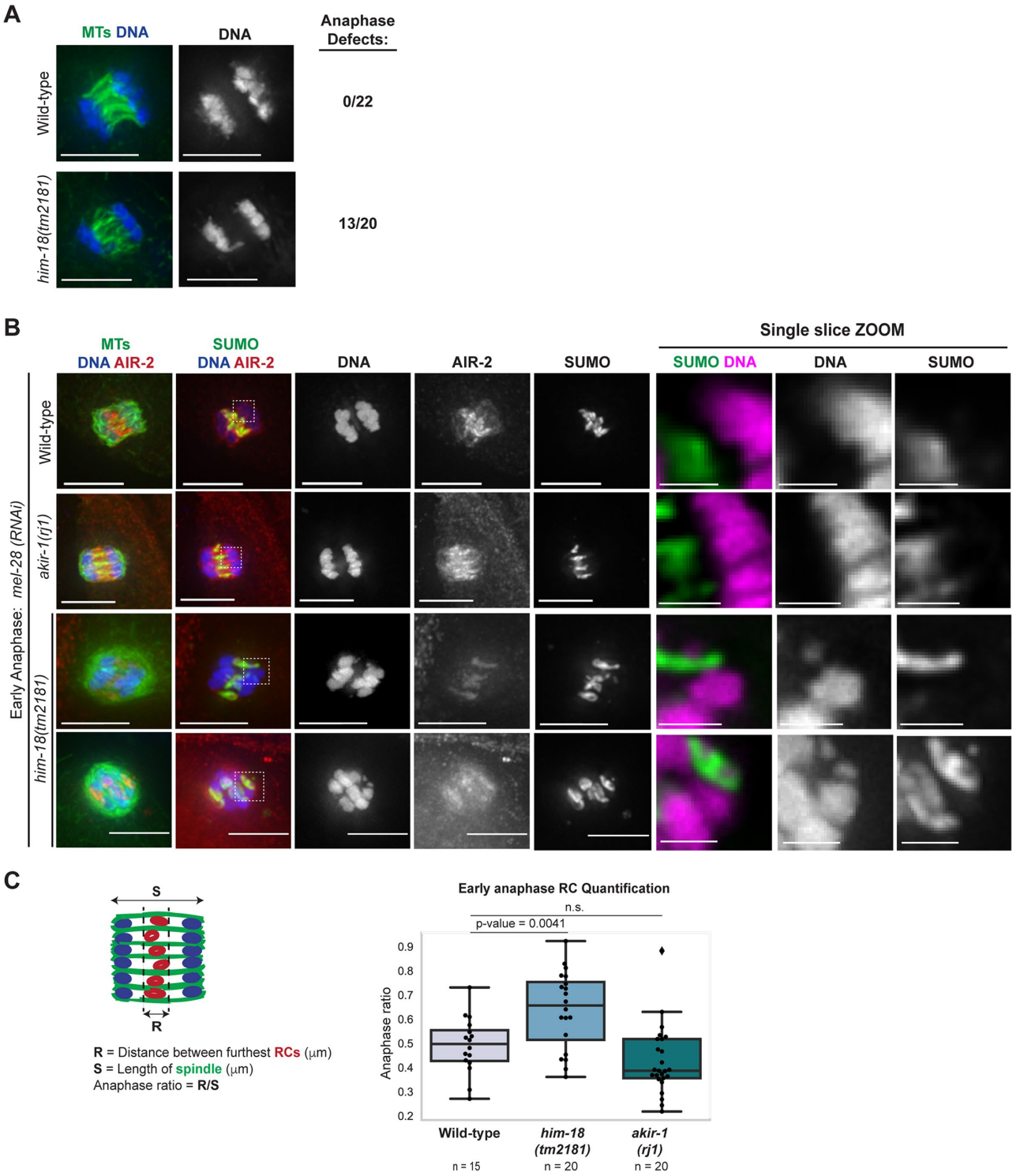

FIGURE 4: Ring complexes are not properly removed from chromosomes in *him-18* mutant anaphases. (A) Wild-type (EU1067) and *him-18(tm2181)* during Anaphase I; shown are DNA (blue) and tubulin (green). Anaphase defects were quantified using sum projections of the DNA channel; *him-18(2181)* mutants had frequent anaphase defects, as previously reported (Saito *et al.*, 2009). (B) Wild-type (EU1067), *akir-1(rj1),* and *him-18(tm2181)* spindles arrested in early Anaphase I using *mel-28(RNAi).* Shown are DNA (blue), AIR-2 (red), tubulin (green, column 1), and SUMO (green, column 2). Single-slice zooms show DNA (magenta) and SUMO (green). While there is a space between SUMO and DNA in wild-type and *akir-1(rj1)* anaphases, indicating that RCs have disengaged from chromosomes, RCs in *him-18(tm2181)* remain associated with chromosomes, looping around the short-arm nubs. (C) Quantification of RC localization following *mel-28(RNAi);* the anaphase ratio was calculated by measuring the distance between the two farthest rings, and then dividing that distance by the pole-to-pole spindle length. RCs in *him-18(tm2181)* spindles occupy a larger fraction of the spindle than in wild-type anaphase ($p = 0.004$; two-tailed Student's *t* test). Scale bars = 5 μm (full images), 1 μm (zooms).

release of cohesion in this domain could theoretically serve to facilitate the release of these subloops. Consistent with this interpretation, we found that RCs are properly released from chromosomes in *akir-1* mutants (Figure 4, B and C); since RC organization is largely normal in this mutant (Figure 2A), removal of cohesin from the short-arm domain should serve to detach the RCs properly. In contrast, the release of cohesin appears to be insufficient for RC release in *him-18* mutants. We infer that this is because *him-18(tm2181)* bivalents never form a mature crossover, and therefore the homologs are physically linked by Holliday Junction intermediates instead of short-arm cohesin (Saito *et al.*, 2009; Figure 2A). This likely interferes with both RC release and homolog resolution, causing the segregation errors seen in later stages of anaphase in previous work (Saito *et al.*, 2009) and in the current study (Figure 4A).

Notably, we were unable to observe any distinctions in *him-18(tm2181)* bivalent segregation that may indicate differential behavior between "stacked" and "cracked" bivalents. We carefully examined *him-18(tm2181), mel-28(RNAi)* anaphase spindles, to see if we could find instances where both homologs of an individual bivalent moved to the same pole; this is an outcome we predicted might occur for monooriented "cracked" bivalents, since both lobes were pointing in the same direction at metaphase. However, we were unable to find clear examples of this segregation pattern. One possibility is that we inadvertently overlooked chromosomes exhibiting this behavior; since chromosomes are clustered close together at each pole, we may have been unable to identify them properly. However, another intriguing possibility is that the monoorientation of "cracked" bivalents is somehow resolved before anaphase, suggesting a unique mechanism of monoorientation correction in holocentric systems.

Summary and impact

Taken together, our work has yielded important new insights into the structure and behavior of the RC during meiosis. First, we discovered that RC components do not solely encircle the outside of the Meiosis I bivalent but also weave through the internal midbivalent region, forming subloops within the larger structure. Based on our data we propose that (1) these subloops encircle the domains where cohesins link sister chromatids at the short-arm interface, (2) release of cohesin by separase in this domain could act to disengage these subloops from the bivalent, and (3) this release is essential to remove the RCs from bivalents in Anaphase I, allowing homologs to segregate efficiently.

In mouse meiosis, Aurora B (the homolog of AIR-2 in *C. elegans*) and the closely related meiosis-specific kinase Aurora C are well-established cell-cycle mediators (Nguyen and Schindler, 2017). Although Aurora B/C does not form a ring structure, these kinases localize to chromosomes and promote cohesion loss through direct phosphorylation of the cohesin protein REC-8 (Nikalayevich *et al.*, 2022). Our findings suggest a potential way that AIR-2 may similarly regulate proper cohesin loss in holocentric *C. elegans* bivalents. In this system, cohesin is lost along the short-arm interface in Meiosis I, and localization of AIR-2 to this axis is required for the correct pattern of cohesin loss (Kaitna *et al.*, 2002; Rogers *et al.*, 2002; Martinez-Perez *et al.*, 2008; Tzur *et al.*, 2012); AIR-2 phosphorylates the cohesin subunit REC-8 in this domain, likely to promote cleavage by separase (Ferrandiz *et al.*, 2018). We propose that by wrapping AIR-2 around short-arm cohesin in the form of subloops, the holocentric bivalent is poised to release cohesion in those domains. Specifically, this population of subloop AIR-2, by forming an internal domain within the bivalent, can efficiently access and phosphorylate cohesin for cleavage by separase. Although we do not yet understand the physical nature of the connection between the RC and the chromosome, this is an intriguing question now primed for further exploration.

Furthermore, we found that both the structure of the RC and its placement at the center of the bivalent are essential for chromosome congression. In other systems, chromosomes achieve biorientation when duplicated kinetochores establish end-on attachments to microtubules emanating from opposite spindle poles; these attachments distribute tension evenly across the chromosome and ensure proper chromosome alignment and segregation. Despite not forming end-on attachments, we show here that chromosome biorientation is still required in *C. elegans* oocytes. While properly bioriented ("stacked") bivalents in the *him-18* mutant exhibited normal chromosome migration, bivalents of the same mutant background that were monooriented ("cracked"), with the RC on one side of the bivalent, had a reduced polar ejection force. This finding reveals the value of a proper distribution of the bivalent mass relative to the RC in facilitating chromosome movement, further highlighting the importance of proper chromosome structure during meiosis. Interestingly, the observation that lateral microtubules bundles served to guide most of the fragile *him-18(tm2181)* bivalents into a stacked configuration supports a role for these bundles in facilitating chromosome biorientation, as previously hypothesized (Wignall and Villeneuve, 2009). By imposing spatial constraints on the chromosome arms, laterally associated microtubule bundles could ensure that the two homologs are pointed toward opposite spindle poles, thus increasing the fidelity of segregation even in mutants with defective chromosome structure. Future studies of other meiotic chromosome structure mutants could shed additional light on how microtubules interface with chromosomes to ensure accurate segregation in this system.

MATERIALS AND METHODS

Request a protocol through *Bio-protocol*.

Worm maintenance

All worms were grown and maintained at 15°C unless otherwise noted. AV335 worms were grown at 15°C and moved to the restrictive temperature of 25°C 5 h before experimentation to induce metaphase arrest and ring stretching.

Strains used in this study:

N2 (Bristol)

AV335: *emb-27(g48)II; unc-119(ed3) ruIs32[unc-119(+) pie-1^{promoter}::GFP::H2B]III; ruIs57[unc-119(+) pie-1^{promoter}::GFP::tubulin]*

CV98: *him-18(tm2181)/qC1 [dpy-19(e1259) glp-1(q339) qIs26] III*

EU1067: *unc-119(ed3) ruIs32[unc-119(+) pie-1^{promoter}::GFP::H2B] III; ruIs57[unc-119(+) pie-1 ^{promoter}::GFP::tubulin]*

SSM356: *akir-1(rj1)I*

Immunofluorescence

Immunofluorescence was performed as previously described (Wolff *et al.*, 2022a). Briefly, worms were picked into a drop of M9 buffer on a poly-L-lysine slide and then dissected to release oocytes. Slides were then frozen in liquid nitrogen for 10 min, and the coverslip was quickly removed. Embryos were fixed for 35 min in –20°C methanol, rehydrated in PBS, and blocked in AbDil (PBS plus 4% BSA, 0.1% Triton X-100, 0.02% Na-Azide).

Primary antibodies were diluted in AbDil and incubated overnight at 4°C. Secondary antibodies were diluted in AbDil and incubated for 2 h at room temperature. Hoechst 33342 (Invitrogen) was diluted

1:1000 in PBST (PBS + 0.1% Triton X-100) and incubated for 10 min at room temperature. Slides were washed with PBST between antibody incubations and mounted in 0.5% *p*-phenylenediamine in 90% glycerol, 20 mM Tris, pH 8.8. Slides used for OMX/superresolution imaging were prepared using the same protocol except that they were mounted using VectaShield Mounting Media.

The following antibodies were used for immunofluorescence: rabbit anti-AIR-2 (1:1000; gift from Jill Schumacher), mouse anti-α-tubulin-FITC (1:500; Sigma), mouse anti-SUMO (1:500, gift from Federico Pelisch), rabbit anti-BUB-1 (1:2000; Davis-Roca *et al.*, 2018), rabbit anti-KLP-19 (1:2500; Divekar *et al.*, 2021), rabbit anti-SEP-1 (1:200, gift from Andy Golden), and rabbit anti-ASPM-1 (1:5000, gift from Arshad Desai). The CLS-2 antibody was generated by Covance in rabbits using recombinant full-length GST-CLS-2; serum was then affinity purified and the antibody was used at 1:1000.

Microscopy

Most of the imaging was performed on a DeltaVision Core microscope with a 100× objective (NA = 1.4; Applied Precision). This microscope is housed in the Northwestern Biological Imaging Facility supported by the NU Office for Research. Slides were imaged at room temperature and image stacks were obtained at 0.2-µm *z*-steps and deconvolved (ratio method, 15 cycles) using SoftWoRx (Applied Precision). All images in this study were displayed as full maximum intensity projections of data stacks encompassing the entire spindle structure unless otherwise noted.

Images in Figure 1, B and C (denoted as superresolution) were acquired on an OMX 3D-SIM microscope (Applied Precision) with an Olympus 100× UPlanSApo objective (NA = 1.4) in the Center for Advanced Microscopy at Northwestern University. Images were captured at 0.125-µm *z*-steps and processed using SoftWoRx (Applied Precision), IMARIS 3D imaging software (Bitplane), and FIJI.

RNAi

RNAi was performed as described by Wolff *et al.* (2022a). Briefly, from a feeding library (Fraser *et al.*, 2000; Kamath *et al.*, 2003), individual RNAi clones were grown overnight at 37°C in LB with 100 µg/ml ampicillin. Overnight cultures were spun down and plated on NGM (nematode growth media) plates containing 100 µg/ml ampicillin and 1 mM IPTG, and then plates were dried overnight. Worm strains were synchronized by bleaching gravid adults and hatching overnight without food. Most RNAi was performed by moving synchronized L1s onto RNAi plates, but for partial *knl-1(RNAi)*, worms were moved onto plates 48 h before dissection, since longer incubation times resulted in germline defects.

Chromosome congression quantification (metaphase plate and bivalent migration ratios)

For Figure 3A, metaphase arrest was induced in wild-type, *him-18(tm2181)*, and *akir-1(rj1)* worms using *emb-30(RNAi)* and *z*-stacks were obtained as described in *Microscopy*. Three-dimensional renderings of metaphase spindles were generated using Imaris. The length of the spindle was determined by rotating the spindle into a side view and measuring the distance between the outermost edges of poles. For the metaphase plate ratios, the SUMO ring closest to each pole was identified and the distance between them was measured on an axis parallel to the pole-to-pole spindle axis. The metaphase ratio was calculated by dividing this distance by the spindle length. For the bivalent migration ratios, the distance between each SUMO ring and its nearest pole was measured. The bivalent migration ratio was calculated by dividing this distance by spindle length. Statistical significance was assessed using a two-tailed Student's *t* test.

Chromosome migration distances on monopolar spindles

Since the kinesin-12 family motor KLP-18 is required for sorting microtubule minus ends outward during spindle assembly, depletion of this motor results in the formation of a single central monopole (Wignall and Villeneuve, 2009; Wolff *et al.*, 2016, 2022b). For Figure 3C, monopolar spindles were therefore generated in wild-type, *him-18(tm2181)*, and *akir-1(rj1)* worms using *klp-18(RNAi)* and *z*-stacks were obtained as described in *Microscopy*. Three-dimensional renderings of monopolar spindles were generated using Imaris. The center of each monopole was determined using the "Surface" tool in Imaris to create a mask of the ASPM-1 volume and assign a center point to this shape. Chromosome migration distances were determined by measuring the distance between the monopole center and the poleward surface of each bivalent. Statistical significance was assessed using a two-tailed Student's *t* test.

Anaphase quantifications

For Figure 4C, early anaphase arrest was induced in wild-type, *him-18(tm2181)*, and *akir1(rj1)* worms using *mel-28(RNAi)* and *z*-stacks were obtained as described in *Microscopy*. Three-dimensional renderings of early anaphase spindles were generated using Imaris. The length of the spindle was determined by rotating the spindle into a side view and measuring the distance between the outermost edge of each pole. The most poleward SUMO signal was identified for each spindle half, and the distance between these signals was measured on an axis parallel to the pole-to-pole distance. The anaphase ratio was calculated by dividing the SUMO-occupied distance by the spindle length. Statistical significance was assessed using a two-tailed Student's *t* test. For Figure 4A, anaphase defects were defined as either chromatin strings or entire homologs that were distinguishable from the two segregating DNA masses and lagging closer to the spindle midzone.

ACKNOWLEDGMENTS

We would like to thank Tom Hope's lab at Northwestern University for providing training and access to the OMX superresolution microscope and Keila Torre-Santiago for help with acquisition of the image in Figure 1C. We would also like to thank members of the Wignall lab and the WiLa ICB for support and guidance, particularly Gabe Cavin-Meza, Emily Czajkowski, Jordy Martinez, and Juhi Narula for providing feedback on the manuscript. We are grateful to Arshad Desai, Andy Golden, Federico Pelisch, and Jill Schumacher for antibodies and the *Caenorhabditis* Genetics Center, funded by the NIH Office of Research Infrastructure Programs (P40 OD010440), for strains. This work was supported by Cellular and Molecular Basis of Disease (CMBD) Training Grant NIH T32 GM00806 (to H.E.H.) and NIH R01GM124354 (to S.M.W.). Microscopy was performed at the Biological Imaging Facility at Northwestern University, supported by the Chemistry for Life Processes Institute, the NU Office for Research, and the Department of Molecular Biosciences.

REFERENCES

Carlton PM, Davis RE, Ahmed S (2022). Nematode chromosomes. Genetics 221.

Clemons AM, Brockway HM, Yin Y, Kasinathan B, Butterfield YS, Jones SJ, Colaiacovo MP, Smolikove S (2013). Akirin is required for diakinesis bivalent structure and synaptonemal complex disassembly at meiotic prophase I. Mol Biol Cell 24, 1053–1067.

Connolly AA, Sugioka K, Chuang CH, Lowry JB, Bowerman B (2015). KLP-7 acts through the Ndc80 complex to limit pole number in *C. elegans* oocyte meiotic spindle assembly. J Cell Biol 210, 917–932.

Davis-Roca AC, Divekar NS, Ng RK, Wignall SM (2018). Dynamic SUMO remodeling drives a series of critical events during the meiotic divisions in *Caenorhabditis elegans*. PLoS Genet 14, e1007626.

Davis-Roca AC, Muscat CC, Wignall SM (2017). *Caenorhabditis elegans* oocytes detect meiotic errors in the absence of canonical end-on kinetochore attachments. J Cell Biol 216, 1243–1253.
de Carvalho CE, Zaaijer S, Smolikov S, Gu Y, Schumacher JM, Colaiacovo MP (2008). LAB-1 antagonizes the Aurora B kinase in *C. elegans*. Genes Dev 22, 2869–2885.
Divekar NS, Davis-Roca AC, Zhang L, Dernburg AF, Wignall SM (2021). A degron-based strategy reveals new insights into Aurora B function in *C. elegans*. PLoS Genet 17, e1009567.
Dumont J, Oegema K, Desai A (2010). A kinetochore-independent mechanism drives anaphase chromosome separation during acentrosomal meiosis. Nat Cell Biol 12, 894–901.
Ferrandiz N, Barroso C, Telecan O, Shao N, Kim HM, Testori S, Faull P, Cutillas P, Snijders AP, Colaiacovo MP, *et al*. (2018). Spatiotemporal regulation of Aurora B recruitment ensures release of cohesion during *C. elegans* oocyte meiosis. Nat Commun 9, 834.
Fraser AG, Kamath RS, Zipperlen P, Martinez-Campos M, Sohrmann M, Ahringer J (2000). Functional genomic analysis of *C. elegans* chromosome I by systematic RNA interference. Nature 408, 325–330.
Gray S, Cohen PE (2016). Control of meiotic crossovers: From double-strand break formation to designation. Annu Rev Genet 50, 175–210.
Hattersley N, Cheerambathur DK, Moyle MW, Stefanutti M, Richardson A, Lee K, Dumont J, Oegema K, Desai A (2016). A nucleoporin docks protein phosphatase 1 to direct meiotic chromosome segregation and nuclear assembly. Dev Cell 38, 463–477.
Hollis JA, Glover ML, Schlientz AJ, Cahoon CK, Bowerman B, Wignall SM, Libuda DE (2020). Excess crossovers impede faithful meiotic chromosome segregation in *C. elegans*. PLoS Genet 16, e1009001.
Kaitna S, Pasierbek P, Jantsch M, Loidl J, Glotzer M (2002). The aurora B kinase AIR-2 regulates kinetochores during mitosis and is required for separation of homologous chromosomes during meiosis. Curr Biol 12, 798–812.
Kamath RS, Fraser AG, Dong Y, Poulin G, Durbin R, Gotta M, Kanapin A, Bot NL, Moreno S, Sohrmann M, *et al*. (2003). Systematic functional analysis of the *Caenorhabditis elegans* genome using RNAi. Nature 421, 231–237.
Laband K, Borgne RL, Edwards F, Stefanutti M, Canman JC, Verbavatz JM, Dumont J (2017). Chromosome segregation occurs by microtubule pushing in oocytes. Nat Commun 8, 1499.
Martinez-Perez E, Schvarzstein M, Barroso C, Lightfoot J, Dernburg AF, Villeneuve AM (2008). Crossovers trigger a remodeling of meiotic chromosome axis composition that is linked to two-step loss of sister chromatid cohesion. Genes Dev 22, 2886–2901.
Monen J, Maddox PS, Hyndman F, Oegema K, Desai A (2005). Differential role of CENP-A in the segregation of holocentric *C. elegans* chromosomes during meiosis and mitosis. Nat Cell Biol 7, 1248–1255.
Mullen TJ, Davis-Roca AC, Wignall SM (2019). Spindle assembly and chromosome dynamics during oocyte meiosis. Curr Opin Cell Biol 60, 53–59.
Mullen TJ, Wignall SM (2017). Interplay between microtubule bundling and sorting factors ensures acentriolar spindle stability during *C. elegans* oocyte meiosis. PLoS Genet 13, e1006986.
Muscat CC, Torre-Santiago KM, Tran MV, Powers JA, Wignall SM (2015). Kinetochore-independent chromosome segregation driven by lateral microtubule bundles. eLife 4, e06462.
Nabeshima K, Villeneuve AM, Colaiacovo MP (2005). Crossing over is coupled to late meiotic prophase bivalent differentiation through asymmetric disassembly of the SC. J Cell Biol 168, 683–689.
Nguyen AL, Schindler K (2017). Specialize and divide (twice): Functions of three aurora kinase homologs in mammalian oocyte meiotic maturation. Trends Genet 33, 349–363.
Nikalayevich E, El Jailani S, Dupre A, Cladiere D, Gryaznova Y, Fosse C, Buffin E, Touati SA, Wassmann K (2022). Aurora B/C-dependent phosphorylation promotes Rec8 cleavage in mammalian oocytes. Curr Biol 32, 2281–2290.e2284.
Pelisch F, Bel Borja L, Jaffray EG, Hay RT (2019). Sumoylation regulates protein dynamics during meiotic chromosome segregation in *C. elegans* oocytes. J Cell Sci
Pelisch F, Tammsalu T, Wang B, Jaffray EG, Gartner A, Hay RT (2017). A SUMO-dependent protein network regulates chromosome congression during oocyte meiosis. Mol Cell 65, 66–77.
Redemann S, Lantzsch I, Lindow N, Prohaska S, Srayko M, Muller-Reichert T (2018). A switch in microtubule orientation during *C. elegans* meiosis. Curr Biol 28, 2991–2997 e2992.
Rogers E, Bishop JD, Waddle JA, Schumacher JM, Lin R (2002). The aurora kinase AIR-2 functions in the release of chromosome cohesion in *Caenorhabditis elegans* meiosis. J Cell Biol 157, 219–229.
Romano A, Guse A, Krascenicova I, Schnabel H, Schnabel R, Glotzer M (2003). CSC-1: a subunit of the Aurora B kinase complex that binds to the survivin-like protein BIR-1 and the incenp-like protein ICP-1. J Cell Biol 161, 229–236.
Saito TT, Youds JL, Boulton SJ, Colaiacovo MP (2009). *Caenorhabditis elegans* HIM-18/SLX-4 interacts with SLX-1 and XPF-1 and maintains genomic integrity in the germline by processing recombination intermediates. PLoS Genet 5, e1000735.
Sato-Carlton A, Nakamura-Tabuchi C, Chartrand SK, Uchino T, Carlton PM (2018). Phosphorylation of the synaptonemal complex protein SYP-1 promotes meiotic chromosome segregation. J Cell Biol 217, 555–570.
Schumacher JM, Golden A, Donovan PJ (1998). AIR-2: An Aurora/Ipl1-related protein kinase associated with chromosomes and midbody microtubules is required for polar body extrusion and cytokinesis in *Caenorhabditis elegans* embryos. J Cell Biol 143, 1635–1646.
Schvarzstein M, Wignall SM, Villeneuve AM (2010). Coordinating cohesion, co-orientation, and congression during meiosis: lessons from holocentric chromosomes. Genes Dev 24, 219–228.
Tzur YB, Egydio de Carvalho C, Nadarajan S, Van Bostelen I, Gu Y, Chu DS, Cheeseman IM, Colaiacovo MP (2012). LAB-1 targets PP1 and restricts Aurora B kinase upon entrance into meiosis to promote sister chromatid cohesion. PLoS Biol 10, e1001378.
von Diezmann L, Rog O (2021). Let's get physical—mechanisms of crossover interference. J Cell Sci 134, jcs255745.
Wignall SM, Villeneuve AM (2009). Lateral microtubule bundles promote chromosome alignment during acentrosomal oocyte meiosis. Nat Cell Biology 11, 839–844.
Wolff ID, Divekar NS, Wignall SM (2022a). Methods for investigating cell division mechanisms in *C. elegans*. Methods Mol Biol 2415, 19–35.
Wolff ID, Hollis JA, Wignall SM (2022b). Acentrosomal spindle assembly and maintenance in *C. elegans* oocytes requires a kinesin-12 non-motor microtubule interaction domain. Mol Biol Cell mbcE22020056.
Wolff ID, Tran MV, Mullen TJ, Villeneuve AM, Wignall SM (2016). Assembly of C. elegans acentrosomal spindles occurs without evident MTOCs and requires microtubule sorting by KLP-18/kinesin-12 and MESP-1. Mol Biol Cell 27, 3122–3131.